

Density-Independent Glassy Behavior in the High-Density Phase of Motility-Induced Phase Separation

Toranosuke Umemura,¹ Issei Sakai,¹ and Takuma Akimoto^{1,*}

¹*Department of Physics and Astronomy, Tokyo University of Science, Noda, Chiba 278-8510, Japan*
(Dated: June 17, 2025)

We investigate the nonequilibrium dynamics of active matter using a two-dimensional active Brownian particles model. In these systems, self-propelled particles undergo motility-induced phase separation (MIPS), spontaneously segregating into dense and dilute phases. We find that in the high-density phase, local particle mobility exhibits glassy behavior, with diffusivity remaining unchanged despite variations in the global system density. As global density increases further, the system undergoes a transition to a solid-like state through this glassy phase. These findings provide insights into nonequilibrium phase transitions in active matter, revealing a robust glassy phase en route to solidification, and may guide future studies in both synthetic and biological active systems.

Active matter consists of self-propelled particles or individual units that consume energy to produce movement or exert forces, leading to spontaneous motion and collective behavior [1–5]. Unlike passive matter, which remains in thermodynamic equilibrium and moves only due to external forces or thermal fluctuations, active matter continuously consumes energy to drive self-propulsion and collective motion. Examples include synthetic Janus particles [6, 7], motile bacterial cells [8], and animal groups like bird flocks or fish schools [9–11], all of which display self-organization and collective dynamics. These systems exhibit diverse collective phenomena, offering fundamental insights into nonequilibrium statistical mechanics.

One of the most striking behaviors in active matter is motility-induced phase separation (MIPS) [12], where self-propelled particles segregate into dense and dilute phases due to the interplay between activity and interparticle interactions. Unlike equilibrium phase separation, which typically requires attractive forces, MIPS occurs even in purely repulsive systems and has been observed in both simulations and experiments [13–15]. Hydrodynamic interactions are known to influence MIPS, sometimes suppressing phase separation [16]. While MIPS has been widely studied, particularly regarding cluster formation and phase behavior, the dynamical properties of the high-density phase, especially in relation to glassy dynamics, remain an open question [17].

Diffusion in active matter systems is a key property that governs nonequilibrium transport and phase behavior. The long-time diffusion coefficients in the active suspension decrease with increasing the density [17, 18], and at densities where MIPS occurs, they drop sharply [17]. Within the high-density phase of MIPS, the mean squared displacement (MSD) is suppressed compared to single-particle systems and exhibits subdiffusive, superdiffusive, and normal diffusive behaviors at short, intermediate, and long times, respectively [19]. While MIPS has been widely studied [17], the long-time diffusion properties of active particles in the high-density phase remain unclear. Unlike passive systems, where

caging effects lead to subdiffusive behavior in glasses, self-propulsion in active systems introduces competing effects that may enhance or suppress diffusion [18, 20]. Understanding how diffusion behaves in the high-density phase of MIPS is crucial for distinguishing glassy states from solid-like states and characterizing nonequilibrium phase transitions.

To this end, we employ a two-dimensional active Brownian particles (ABPs) model [3, 21, 22] to analyze the nonequilibrium dynamics across a range of global system densities, including those exhibiting MIPS. Our study aims to determine whether diffusivity and structural order remain invariant or change with increasing global density and to understand how the system transitions from MIPS to a solid-like state, potentially through a glassy phase. To characterize these behaviors, we use the bond-orientational order parameter and mean squared interparticle distance (MSID), which quantify local structural order and particle motion in the high-density phase, respectively. Our findings reveal the persistence of glassy states in active systems and clarify the pathway to solidification in nonequilibrium matter.

Model.—In the model, the system consists of N self-propelled particles confined to a two-dimensional domain. Each particle's motion is governed by an overdamped Langevin equation

$$\gamma \dot{\mathbf{r}}_i(t) = \boldsymbol{\chi}_i(t) + \gamma s \boldsymbol{\omega}_i(t) - \nabla_i \sum_{j \neq i} \phi(|\mathbf{r}_{ij}|), \quad (1)$$

where γ is the friction constant, $\mathbf{r}_i(t) = (x_i(t), y_i(t))$ represents the position of particle i at time t , $\mathbf{r}_{ij} = \mathbf{r}_i - \mathbf{r}_j$ represents the relative position vector between particles i and j , and s is the constant speed of self-propulsion. The term $\boldsymbol{\chi}_i(t)$ represents thermal fluctuations described by two-dimensional white Gaussian noise, satisfying $\langle \boldsymbol{\chi}_i(t) \rangle = 0$ and $\langle \boldsymbol{\chi}_i(t) \boldsymbol{\chi}_j(t') \rangle = 2k_B T \gamma \delta(t - t') \mathbf{1}_{ij}$. Here, k_B denotes the Boltzmann constant, and T is the absolute temperature. The unit vector $\boldsymbol{\omega}_i(t) = (\cos \theta_i(t), \sin \theta_i(t))$ determines the particle's

orientation, which evolves according to

$$\tilde{\gamma}\dot{\theta}_i(t) = \xi_i, \quad (2)$$

where $\tilde{\gamma}$ is the rotational friction constant, and ξ_i is white Gaussian noise with $\langle \xi_i(t) \rangle = 0$ and $\langle \xi_i(t)\xi_j(t') \rangle = 2k_B T \tilde{\gamma} \delta(t-t') \delta_{ij}$. In the low-Reynolds number, the relation between γ and $\tilde{\gamma}$ is $\tilde{\gamma} = \gamma \sigma^2 / 3$. This noise represents the random reorientation of active particles and is independent of the translational thermal fluctuations.

The interaction between particles is modeled using the Weeks-Chandler-Andersen (WCA) potential [23–30], a purely repulsive potential given by

$$\phi(r_{ij}) = \begin{cases} 4\varepsilon \left[\left(\frac{\sigma}{r_{ij}} \right)^{12} - \left(\frac{\sigma}{r_{ij}} \right)^6 \right] + \varepsilon & (r_{ij} < 2^{1/6}\sigma) \\ 0 & \text{otherwise,} \end{cases} \quad (3)$$

where σ represents the particle diameter, ε is the interaction strength, and $r_{ij} = |\mathbf{r}_{ij}|$ denotes the distance between particle i and j . This potential ensures that particles experience only short-range repulsion, as the interaction is truncated at $r_{ij} = 2^{1/6}\sigma$. Since the force derived from this potential vanishes beyond this cutoff, the interaction remains purely repulsive with no attractive component.

To systematically characterize the system, we introduce two key dimensionless parameters. The first is the Péclet number, defined as $\text{Pe} = 3s\tilde{\gamma}/(\sigma k_B T)$, which quantifies the relative strength of self-propulsion compared to thermal fluctuations of the rotational diffusion. A high Péclet number indicates that the system is dominated by self-propulsion rather than Brownian diffusion. The second important parameter is the global number density, given by $\rho = N/(L_x L_y)$, which represents the overall packing fraction of particles within the simulation domain. Here, L_x and L_y are the system sizes. These parameters allow us to explore the effects of activity and density on the system's phase behavior.

In our simulations, we set the temperature as $k_B T = 1.0$, the particle diameter as $\sigma = 1.0$, and the Péclet number as $\text{Pe} = 120$, with the self-propulsion speed normalized to $s = 1.0$. This relatively high Péclet number ensures that self-propulsion dominates over thermal fluctuations, facilitating the exploration of MIPS [31] and enabling us to investigate the potential emergence of glassy dynamics in the high-density phase. The energy scale is chosen such that $k_B T / \varepsilon = 0.5$, ensuring a balance between thermal fluctuations and interaction strength. The system consists of N ABPs confined in a rectangular domain of size $L_x = 120$ and $L_y = 24$, with periodic boundary conditions. This aspect ratio stabilizes the shape of dense clusters formed through MIPS and suppresses large fluctuations in their center-of-mass motion, enabling a clearer analysis of local particle dynamics.

Cluster Analysis and Phase Stability in MIPS.—We analyze the structural and dynamical properties of the

high-density phase in MIPS by systematically varying the global system density. To characterize the onset of clustering, we compute the fraction of particles within clusters, β_{cluster} , defined as $\beta_{\text{cluster}} = \langle N_{\text{cluster}} \rangle / N$, where N_{cluster} is the number of particles within clusters. A particle is considered to belong to a cluster if it has at least four neighboring particles within a radius σ .

Figure 1 illustrates the variation of β_{cluster} with global density. At low densities ($\rho < 0.6$), $\beta_{\text{cluster}} \approx 0$, indicating no significant clustering. In this phase, the system remains a homogeneous liquid, where nearly all particles move independently. At $\rho = 0.6$, β_{cluster} exhibits large fluctuations because MIPS repeatedly emerges and disappears. This indicates that the high density phase in MIPS is unstable. As the density increases beyond $\rho = 0.7$, β_{cluster} exhibits a sharp increase and only slight fluctuations. These fluctuations are due to the exchange of particles between the high-density and low-density phases. The error bars are smaller than the one at $\rho = 0.6$, suggesting that the high-density phase in MIPS is stable. For $\rho \geq 1.4$, nearly all particles belong to clusters ($\beta_{\text{cluster}} \approx 1$), signifying a transition to a solid-like phase where particle mobility is highly constrained.

Structural Order Analysis via Q_6 Parameter.—Within the high-density phase, we examine structural ordering using the bond-orientational order parameter Q_6 [32, 33], which quantifies the degree of local hexagonal packing. This parameter is computed based on the relative angles between neighboring particles and is defined as

$$Q_6 = \frac{1}{6N} \left\langle \sum_{i=1}^N \sum_{j \neq i, r_{ij} < \sigma} \cos^2(6\alpha_{ij}) \right\rangle. \quad (4)$$

Here, α_{ij} represents the relative angle between particles i and j . The neighboring particles are defined as those for which the particle-pair distance r_{ij} is smaller than σ . The order parameter Q_6 quantifies the extent of hexagonal order in the system. For a perfect hexagonal arrangement, Q_6 approaches 1, indicating a highly ordered structure. Conversely, for a disordered state, Q_6 is close to 0, reflecting the absence of regular particle alignment. This parameter has been widely used in studies of order in liquids and glasses [34].

Figure 1 shows how the order parameter Q_6 varies with the global density. At low densities ($\rho < 0.6$), Q_6 takes small values, indicating that the system lacks overall structural regularity—consistent with a liquid state. As the density increases into the intermediate-density range ($0.6 \leq \rho < 1.4$), Q_6 gradually increases, suggesting the emergence of short-range order. In this regime, local particle arrangements become more regular, but global structural order is not achieved. Moreover, the wide error bars indicate large fluctuations in particle arrangement and the cluster size, suggesting that the system remains structurally disordered at larger scales. As shown in the cluster fraction analysis, MIPS occurs in this density

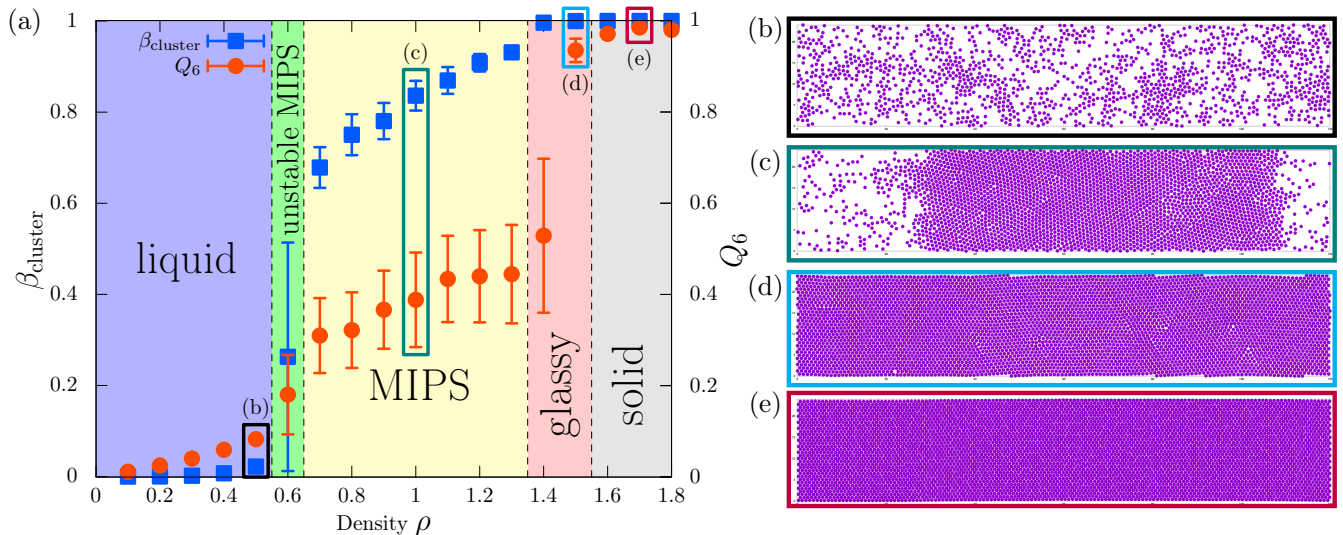


FIG. 1. (a) Density dependence of the cluster fraction β_{cluster} and bond-orientational order parameter Q_6 . Squares and circles show the results of numerical simulations for β_{cluster} and Q_6 , respectively. Error bars represent the standard deviation. The background color indicates the system state: purple (liquid), green (unstable MIPS), yellow (MIPS), light red (glassy), and gray (solid-like). (b)-(e) Representative snapshots at different global densities: $\rho = 0.5, 1.0, 1.5$, and 1.7 .

range, leading to the coexistence of a high-density phase and a low-density phase. At higher densities ($\rho = 1.4$ and 1.5), particles are densely packed throughout the system, yet the error bars still show some spread, indicating that residual fluidity remains—consistent with glassy behavior. As the density increases beyond $\rho = 1.5$, Q_6 approaches unity, and the reduced spread of error bars suggests that the order becomes more stable. Therefore, when $\rho \geq 1.4$, all particles belong to clusters. However, short-range order is unstable for $1.4 \leq \rho < 1.6$, while it becomes stable for $\rho \geq 1.6$.

Probing Glassy Dynamics Using the MSID.—A key feature of glassy behavior is the suppression of long-time particle diffusivity. To assess this in the high-density phase of MIPS, we quantify particle diffusivity and structural constraints. A common method for evaluating diffusivity is to analyze the MSD of a single particle. In the active suspension, the MSD of the entire system and the MSD in the high-density phase of MIPS have been numerically investigated [17, 19]. However, in the high-density phase, the entire cluster undergoes diffusion, leading to collective motion and system-wide fluctuations. As a result, the MSD of an individual particle reflects both its intrinsic motion and the center-of-mass motion of the entire system, making it difficult to isolate true particle diffusivity. This issue is analogous to that observed in small systems such as lipid bilayers, where global fluctuations obscure individual particle motion, complicating diffusivity measurements [35]. To overcome this limitation, we analyze the MSID, which provides a more reliable measure of the relative motion of particle pairs and better captures glassy dynamics in

dense phases. The MSID is defined as

$$\langle \Delta d^2(t) \rangle = \left\langle \frac{1}{N_{\text{pair}}} \sum_{i < j} |\mathbf{r}_{ij}(t) - \mathbf{r}_{ij}(0)|^2 \right\rangle \quad (5)$$

where N_{pair} is the total number of particle pairs that remained continuously in the high-density phase for the entire observation period. By analyzing MSID, we gain deeper insight into the temporal evolution of particle separations, a crucial aspect of the system's dynamical constraints and glassy behavior. Notably, the MSID exhibits a plateau when cage effects confine particles locally, even if the center-of-mass motion of the cluster is not restricted. This distinguishes the relative motion of particles from global drift and highlights the emergence of glassy dynamics within the dense phase. In Ref. [32], the MSID was employed to determine whether the active suspension exhibits solid-like or liquid-like behavior.

Connecting the MSID and MSD under Harmonic Confinement.—In the high-density phase, particles are restricted by their neighbors. In the short-time regime, where particles do not escape their cages, they effectively move independently within their local environments. We approximate their motions as being constrained by independent harmonic potentials and assume that their motions are uncorrelated. Consequently, the MSID can be derived from the MSD via $\langle \Delta d^2(t) \rangle = 2\langle \Delta \mathbf{r}^2(t) \rangle$, where $\Delta \mathbf{r}(t) = \mathbf{r}(t) - \mathbf{r}(0)$ is the displacement vector.

When the initial positions of the particles are sampled from the steady state, the MSD of an ABP in a harmonic

potential is given by [36, 37]

$$\langle \Delta \mathbf{r}^2(t) \rangle = \frac{4k_B T}{\kappa(\rho_{\text{HD}})} \left[1 - e^{-t/\tau_k} \right] + \frac{2s^2 \tau_k^2 \tau_R^2}{\tau_R + \tau_k} \left[1 - \frac{\tau_R e^{-t/\tau_R} - \tau_k e^{-t/\tau_k}}{\tau_R - \tau_k} \right], \quad (6)$$

where $\kappa(\rho_{\text{HD}})$ is the effective spring constant used to approximate the confining effects of neighboring particles, parameterized by the local density ρ_{HD} in the high-density phase [See Supplemental Material]. Here, $\tau_k = \gamma/\kappa(\rho_{\text{HD}})$ is the characteristic relaxation time for the particle's motion in the harmonic potential, and $\tau_R = \tilde{\gamma}/k_B T$ is the rotational relaxation time of the particle, with $\tau_k \ll \tau_R$. The MSD initially grows linearly with time at short times ($t \ll \tau_k$), consistent with free diffusion. At intermediate times ($t \sim \tau_k$), the MSD reaches its first plateau, corresponding to the particle being trapped by the harmonic potential due to thermal fluctuations. At longer times ($\tau_k \ll t \ll \tau_R$), the MSD remains at this plateau as the particle's orientation remains relatively constant. Finally, at times comparable to or greater than τ_R , the rotational diffusion of the propulsion direction allows the particle to explore new configurations, leading to an additional contribution to the MSD from self-propulsion. This contribution creates a second plateau associated with the rotational fluctuations of the particle's propulsion direction.

MSID Behavior in the MIPS Regime ($0.7 \leq \rho < 1.4$).—At short times ($t \ll \tau_k$), the MSID increases linearly with time, consistent with free diffusion where interparticle interactions have minimal influence. The relationship for short times is given by

$$\langle \Delta d^2(t) \rangle \sim \frac{8k_B T}{\gamma} t, \quad (7)$$

which follows from the fact that for two-dimensional Brownian motion, the MSD of a single particle is $4k_B T t/\gamma$. Since MSID measures the displacement between two particles, rather than an individual one, the factor is doubled, leading to Eq. (7).

At intermediate times ($\tau_k \ll t \ll \tau_R$), interparticle interactions constrain particle motion, leading to the emergence of a plateau in $\langle \Delta d^2(t) \rangle$, exhibiting behavior similar to that of a glassy system [38, 39]. For $t/\tau_k \gg 1$ and $t/\tau_R \ll 1$, Eq. (6) is given by $\langle \Delta \mathbf{r}^2(t) \rangle \cong 4k_B T/\kappa(\rho_{\text{HD}})$. Thus, the MSID at the plateau is expressed as

$$\langle \Delta d^2(t) \rangle \cong \frac{8k_B T}{\kappa(\rho_{\text{HD}})}. \quad (8)$$

This relation coincides with the long-time limit of the MSID for Brownian particles in a harmonic potential. The agreement arises because the system is observed prior to the onset of rotational relaxation, where the contribution from ballistic motion remains negligible.

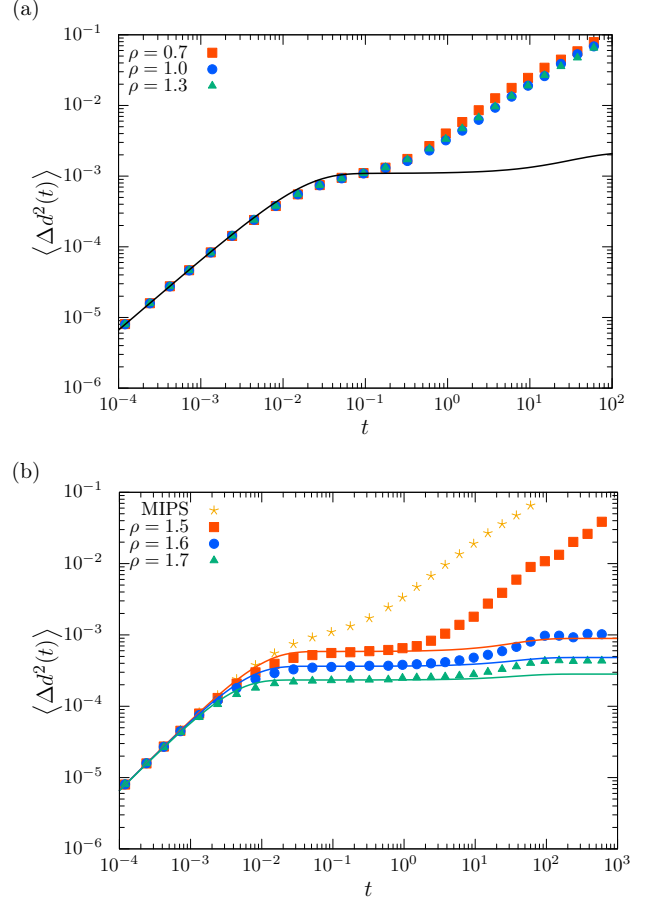


FIG. 2. (a) Mean squared interparticle distance (MSID) in the high-density phase of MIPS for different global density ($\rho = 0.7, 1.0$, and 1.3). Squares, circles, and triangles correspond to the numerical simulation results for $\rho = 0.7, 1.0$, and 1.3 , respectively. The solid line represents Eq. (6) with $\rho_{\text{HD}} = 1.38$, the density of the high-density phase obtained from the numerical simulations. (b) MSID at higher global densities ($\rho = 1.5, 1.6$, and 1.7). Squares, circles, and triangles correspond to the numerical simulation results for $\rho = 1.5, 1.6$, and 1.7 , respectively. Crosses show the numerical simulation result for the high-density phase at $\rho = 1.3$ as a reference. The solid lines represent Eq. (6).

MSID Behavior in the Homogeneous High-Density Regime ($\rho \geq 1.4$).—At long times, particles escape their cages [40–42], resulting in an increase in the MSID. This behavior reflects the onset of fluidity within the high-density phase, where particles gradually regain mobility and transition back to diffusive motion. The MSID increases sublinearly, signaling the restoration of diffusion. This transition—from free diffusion at short times to constrained motion at intermediate times, and finally back to diffusion at long times—suggests that the system exhibits glassy behavior.

In MIPS, the system segregates into coexisting dense and dilute phases, and the density of the high-density phase ρ_{HD} typically remains relatively stable, with only

weak dependence on the global system density ρ [19, 31]. Consequently, the MSID plateau remains constant within the high-density phase, regardless of variations in the global system density. As shown in Fig. 2(a), in the range $0.7 \leq \rho < 1.4$ where MIPS occurs, the MSID remains independent of the global system density ρ . This finding suggests that diffusivity in the high-density phase remains unchanged, even as the overall system density increases.

At higher densities, the high-density phase extends throughout the entire system, resulting in a homogeneous phase. Consequently, a clear plateau emerges in the intermediate-time regime of the MSID [see Fig. 2(b)]. At $\rho = 1.5$, the MSID resumes increasing after exhibiting a plateau, indicating persistent particle mobility. This fluid-like behavior is supported by the bond-orientational order parameter analysis. Furthermore, the time evolution of the MSID—characterized by an initial growth, a plateau, and a subsequent increase—suggests that the system exhibits glassy dynamics in the range $1.4 \leq \rho < 1.6$. In contrast, for $\rho = 1.6$ and 1.7 , the MSID exhibits a slight increase followed by the emergence of a second plateau. This behavior is qualitatively similar to the MSD of an ABP confined in a harmonic potential. In this density regime ($\rho \geq 1.6$), particles are confined by their neighbors, indicating that the system is in a solid-like state. However, the value of the second plateau is larger than that observed for an ABP in a static harmonic potential. In this study, we employed a mean-field approximation by modeling the particle as an ABP confined in a static harmonic potential. In contrast, in the actual system, the confinement can be regarded as a dynamic harmonic potential, where the minimum position fluctuates diffusively. These effects lead to an enhancement of the second plateau in the MSID compared to the static harmonic potential case.

Conclusion.—In this study, we have analyzed the dynamic behavior of ABPs, revealing a transition from a liquid-like state to a glassy state and, ultimately, to a solid-like state as the global system density increases. Key order parameters, such as the Q_6 parameter and the MSID, highlight the crucial role of interparticle interactions in determining the system’s macroscopic state. A notable finding is that the high-density phase in MIPS exhibits persistent glassy behavior, characterized by constrained particle mobility and the absence of long-range order. The MSID remains largely independent of global density, indicating that local diffusivity within the high-density phase is insensitive to changes in the overall system density. These results provide insights into nonequilibrium phase transitions in dense active matter and underscore the stabilizing influence of particle interactions on glassy states. Beyond MIPS, the methodology developed in this study can be applied to more complex active matter systems, including biological systems and synthetic self-propelled particles, contributing to the broader

field of nonequilibrium statistical mechanics.

T.A. was supported by JSPS Grant-in-Aid for Scientific Research (No. C JP21K033920).

* takuma@rs.tus.ac.jp

- [1] J. Toner, Y. Tu, and S. Ramaswamy, Hydrodynamics and phases of flocks, *Ann. Phys. (N. Y.)* **318**, 170 (2005), special Issue.
- [2] E. Lauga and T. R. Powers, The hydrodynamics of swimming microorganisms, *Rep. Prog. Phys.* **72**, 096601 (2009).
- [3] M. C. Marchetti, J. F. Joanny, S. Ramaswamy, T. B. Liverpool, J. Prost, M. Rao, and R. A. Simha, Hydrodynamics of soft active matter, *Rev. Mod. Phys.* **85**, 1143 (2013).
- [4] C. Bechinger, R. Di Leonardo, H. Löwen, C. Reichhardt, G. Volpe, and G. Volpe, Active particles in complex and crowded environments, *Rev. Mod. Phys.* **88**, 045006 (2016).
- [5] G. Gompper, R. G. Winkler, T. Speck, A. Solon, C. Nardin, F. Peruani, H. Löwen, R. Golestanian, U. B. Kaupp, L. Alvarez, T. Kjørboe, E. Lauga, W. C. K. Poon, A. DeSimone, S. Muiños-Landin, A. Fischer, N. A. Söker, F. Cichos, R. Kapral, P. Gaspard, M. Ripoll, F. Sagues, A. Doostmohammadi, J. M. Yeomans, I. S. Aranson, C. Bechinger, H. Stark, C. K. Hemelrijk, F. J. Nedelec, T. Sarkar, T. Aryaksama, M. Lacroix, G. Duclos, V. Yashunsky, P. Silberzan, M. Arroyo, and S. Kale, The 2020 motile active matter roadmap, *J. Phys. Condens. Matter* **32**, 193001 (2020).
- [6] A. Walther and A. H. Müller, Janus particles, *Soft Matter* **4**, 663 (2008).
- [7] N. Vogel, M. Retsch, C.-A. Fustin, A. del Campo, and U. Jonas, Advances in colloidal assembly: The design of structure and hierarchy in two and three dimensions, *Chem. Rev.* **115**, 6265 (2015).
- [8] B. M. Friedrich and F. Jülicher, Chemotaxis of sperm cells, *Proc. Natl. Acad. Sci. U.S.A.* **104**, 13256 (2007).
- [9] I. D. Couzin, J. Krause, N. R. Franks, and S. A. Levin, Effective leadership and decision-making in animal groups on the move, *Nature* **433**, 513 (2005).
- [10] V. Guttal and I. D. Couzin, Social interactions, information use, and the evolution of collective migration, *Proc. Natl. Acad. Sci. U.S.A.* **107**, 16172 (2010).
- [11] D. Sumpter, C. Buhl, D. Biro, and I. Couzin, Information transfer in moving animal groups, *Theory Biosci.* **127**, 177 (2008).
- [12] M. E. Cates and J. Tailleur, Motility-induced phase separation, *Annu. Rev. Condens. Matter Phys.* **6**, 219 (2015).
- [13] J. Palacci, S. Sacanna, A. P. Steinberg, D. J. Pine, and P. M. Chaikin, Living crystals of light-activated colloidal surfers, *Science* **339**, 936 (2013).
- [14] I. Buttinoni, J. Bialké, F. Kümmel, H. Löwen, C. Bechinger, and T. Speck, Dynamical clustering and phase separation in suspensions of self-propelled colloidal particles, *Phys. Rev. Lett.* **110**, 238301 (2013).
- [15] J. Palacci, S. Sacanna, S.-H. Kim, G.-R. Yi, D. J. Pine, and P. M. Chaikin, Light-activated self-propelled colloids, *Philos. Trans. R. Soc. A* **372**, 20130372 (2014).
- [16] R. Matas-Navarro, R. Golestanian, T. B. Liverpool, and

- S. M. Fielding, Hydrodynamic suppression of phase separation in active suspensions, *Phys. Rev. E* **90**, 032304 (2014).
- [17] S. Nayak, P. Bag, P. K. Ghosh, Y. Li, Y. Zhou, Q. Yin, F. Marchesoni, and F. Nori, Diffusion transients in motility-induced phase separation, *Phys. Rev. Res.* **7**, 013153 (2025).
- [18] Y. Fily and M. C. Marchetti, Athermal phase separation of self-propelled particles with no alignment, *Phys. Rev. Lett.* **108**, 235702 (2012).
- [19] G. S. Redner, M. F. Hagan, and A. Baskaran, Structure and dynamics of a phase-separating active colloidal fluid, *Phys. Rev. Lett.* **110**, 055701 (2013).
- [20] J. R. Howse, R. A. L. Jones, A. J. Ryan, T. Gough, R. Vafabakhsh, and R. Golestanian, Self-motile colloidal particles: From directed propulsion to random walk, *Phys. Rev. Lett.* **99**, 048102 (2007).
- [21] J. Stenhammar, A. Tiribocchi, R. J. Allen, D. Marenduzzo, and M. E. Cates, Continuum theory of phase separation kinetics for active Brownian particles, *Phys. Rev. Lett.* **111**, 145702 (2013).
- [22] P. Romanczuk, M. Bär, W. Ebeling, B. Lindner, and L. Schimansky-Geier, Active Brownian particles, *Eur. Phys. J.: Spec. Top.* **202**, 1 (2012).
- [23] J. D. Weeks, D. Chandler, and H. C. Andersen, Role of repulsive forces in determining the equilibrium structure of simple liquids, *J. Chem. Phys.* **54**, 5237 (1971).
- [24] H. C. Andersen, J. D. Weeks, and D. Chandler, Relationship between the hard-sphere fluid and fluids with realistic repulsive forces, *Phys. Rev. A* **4**, 1597 (1971).
- [25] M. K. Nandi and S. M. Bhattacharyya, Microscopic theory of softness in supercooled liquids, *Phys. Rev. Lett.* **126**, 208001 (2021).
- [26] A. Singh and Y. Singh, How attractive and repulsive interactions affect structure ordering and dynamics of glass-forming liquids, *Phys. Rev. E* **103**, 052105 (2021).
- [27] A. Eskandari Nasrabad, Thermodynamic and transport properties of the Weeks–Chandler–Andersen fluid: Theory and computer simulation, *J. Chem. Phys.* **129**, 244508 (2008).
- [28] A. Ahmed and R. J. Sadus, Phase diagram of the weeks-chandler-andersen potential from very low to high temperatures and pressures, *Phys. Rev. E* **80**, 061101 (2009).
- [29] D. Ben-Amotz and G. Stell, Reformulation of Weeks–Chandler–Andersen perturbation theory directly in terms of a hard-sphere reference system, *J. Phys. Chem. B* **108**, 6877 (2004).
- [30] R. Benjamin and J. Horbach, Crystal growth kinetics in Lennard-Jones and Weeks-Chandler-Andersen systems along the solid-liquid coexistence line, *J. Chem. Phys.* **143**, 014702 (2015).
- [31] S. Hermann, P. Krinninger, D. de las Heras, and M. Schmidt, Phase coexistence of active Brownian particles, *Phys. Rev. E* **100**, 052604 (2019).
- [32] J. Bialké, T. Speck, and H. Löwen, Crystallization in a dense suspension of self-propelled particles, *Phys. Rev. Lett.* **108**, 168301 (2012).
- [33] A. Zöttl and H. Stark, Hydrodynamics determines collective motion and phase behavior of active colloids in quasi-two-dimensional confinement, *Phys. Rev. Lett.* **112**, 118101 (2014).
- [34] P. J. Steinhardt, D. R. Nelson, and M. Ronchetti, Bond-orientational order in liquids and glasses, *Phys. Rev. B* **28**, 784 (1983).
- [35] T. Akimoto, E. Yamamoto, K. Yasuoka, Y. Hirano, and M. Yasui, Non-gaussian fluctuations resulting from power-law trapping in a lipid bilayer, *Phys. Rev. Lett.* **107**, 178103 (2011).
- [36] M. Caraglio and T. Franosch, Analytic solution of an active brownian particle in a harmonic well, *Phys. Rev. Lett.* **129**, 158001 (2022).
- [37] S. Halder and M. Khan, Interplay between timescales governs the residual activity of a harmonically bound active brownian particle (2025), arXiv:2505.07265 [cond-mat.soft].
- [38] R. Yamamoto and A. Onuki, Dynamics of highly supercooled liquids: Heterogeneity, rheology, and diffusion, *Phys. Rev. E* **58**, 3515 (1998).
- [39] V. A. Levashov, R. E. Ryltsev, and N. M. Chitchev, Structure of the simple harmonic-repulsive system in liquid and glassy states studied by the triple correlation function, *J. Phys.: Condens. Matter* **33**, 025403 (2020).
- [40] E.-M. Schötz, M. Lanio, J. A. Talbot, and M. L. Manning, Glassy dynamics in three-dimensional embryonic tissues, *J. R. Soc. Interface* **10**, 20130726 (2013).
- [41] L. Berthier, Nonequilibrium glassy dynamics of self-propelled hard disks, *Phys. Rev. Lett.* **112**, 220602 (2014).
- [42] Y. Fily, S. Henkes, and M. C. Marchetti, Freezing and phase separation of self-propelled disks, *Soft Matter* **10**, 2132 (2014).

SUPPLEMENTAL MATERIAL FOR DENSITY-INDEPENDENT GLASSY BEHAVIOR IN THE HIGH-DENSITY PHASE OF MOTILITY-INDUCED PHASE SEPARATION

In our analysis, we approximate the effective interparticle interactions in the high-density phase using a mean-field harmonic potential. The mean-field approach represents the averaged effect of neighboring particles on a given particle. Specifically, this interaction is modeled by a harmonic potential with a spring constant κ , which quantifies the strength of the restoring force that constrains particles near their equilibrium positions. To determine κ , we compare it to the Weeks-Chandler-Andersen (WCA) potential, which describes the short-range repulsive interactions in our system.

The WCA potential is a truncated and shifted form of the Lennard-Jones potential. This potential effectively prevents overlapping of particles while allowing for local fluctuations around the equilibrium separation distance r_{avg} (see Fig. 3). To approximate the spring constant κ , we expand the WCA potential around the equilibrium distance and take the second derivative:

$$\kappa = \left. \frac{d^2 \phi_{\text{WCA}}}{dr^2} \right|_{r=r_{\text{avg}}} . \quad (9)$$

The spring constant is determined by comparing it to the WCA potential and is given by

$$\kappa = [\phi''(r_1 + r_{\text{avg}}) + \phi''(r_2 - r_{\text{avg}})]_{r_1=0, r_2=0} = 1248\varepsilon \frac{\sigma^{12}}{r_{\text{avg}}^{14}} - 336\varepsilon \frac{\sigma^6}{r_{\text{avg}}^8} \quad (10)$$

Here, r_{avg} is the optimal particle distance in the hexagonal close-packed (HCP) structure, which depends on the density ρ .

Consider two independent Brownian particles under harmonic potentials [see Fig. 4]. The equilibrium distance r_{avg} in a HCP structure is determined by the density in the high-density phase ρ_{HD} [see Fig. 3]. In an HCP arrangement, it follows the relation

$$\rho_{\text{HD}} = \frac{3}{\frac{6\sqrt{3}}{4} r_{\text{avg}}^2} . \quad (11)$$

Rearranging this expression, we obtain $r_{\text{avg}} = \sqrt{2/\sqrt{3}\rho_{\text{HD}}}$.

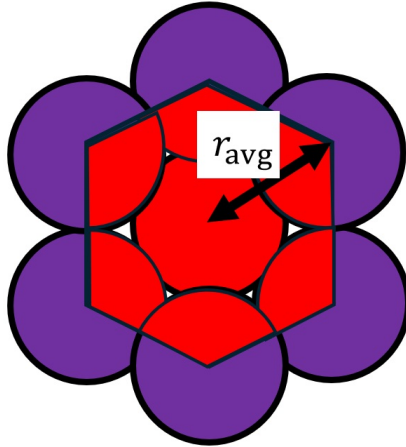


FIG. 3. Hexagonal close-packed structure. r_{avg} is the optimal particle distance in the hexagonal close-packing structure.

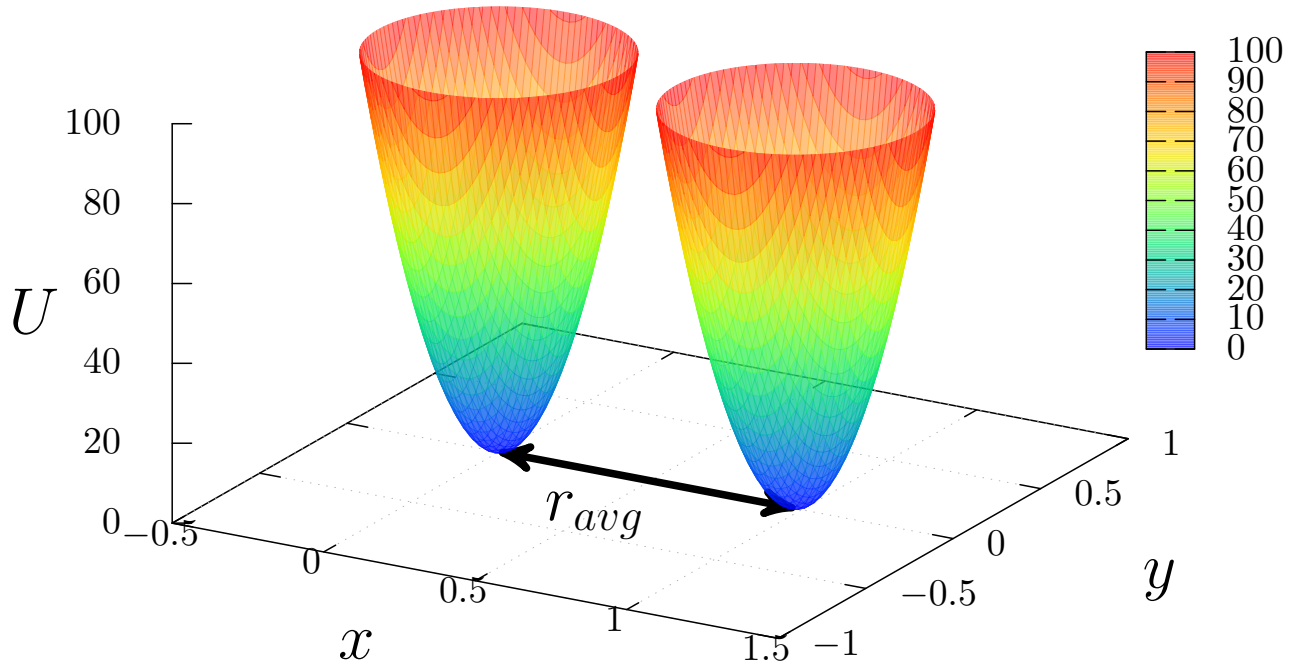


FIG. 4. Two independent harmonic potentials. The distance between the two potential minima is r_{avg} . By approximating the motion of ABPs in the high-density phase to the motion of particles in this potential, the plateau value of the MSID can be calculated.